Electronic Supplementary Material (ESI) for ChemComm.

Metal-Biomolecule Frameworks (BioMOFs): a novel approach for "green" optoelectronic applications

Cristina Martin,[1,2,*] Dries Jonckheere,[3] Eduardo Coutino-Gonzalez,[4] Simon Smolders,[3] Bart Bueken,[3] Carlos Marquez,[3] Andraž Krajnc,[5] Tom Willhammar,[6] Koen Kennes,[1] Oliver Fenwick,[7,8] Fanny Richard,[8] Paolo Samorì,[8] Gregor Mali,[5] Johan Hofkens,[1] Maarten B. J. Roeffaers,[3] Dirk E. De Vos[3]

[1]KU Leuven, Leuven Chem&Tech - Molecular Imaging and Photonics (MIP), Celestijnenlaan 200F post box 2404, 3001 Leuven, Belgium

[2]Unidad nanoCRIB. Centro Regional de Investigaciones Biomédicas, 02071, Albacete, Spain

[3]KU Leuven, Leuven Chem&Tech - Centre for Membrane Separations, Adsorption, Catalysis and Spectroscopy for Sustainable Solutions (cMACS), Celestijnenlaan 200F post box 2454, 3001 Leuven, Belgium

[4]Centro de Investigaciones en Óptica, A. C. Loma del Bosque 115, Colonia Lomas del Campestre, León, Guanajuato 37150, Mexico

[5] Department of Inorganic Chemistry and Technology, National Institute of Chemistry, Hajdrihova 19, 1001 Ljubljana, Slovenia

[6]Department of Materials and Environmental Chemistry, Stockholm University, Svante Arrhenius väg 16C, 106 91 Stockholm, Sweden

[7]Queen Mary University of London, School of Engineering and Materials Science, Mile End Road, London E1 4NS, United Kingdom

[8] University of Strasbourg, CNRS, ISIS UMR 7006, 8 Allée Gaspard Monge, Strasbourg 67000, France

EXPERIMENTAL SECTION

Reagents. Silver nitrate (99.85%), adenine (99%), N,N-dimethylformamide (DMF) (>99%) and zinc acetate dihydrate (>98%) were purchased from Acros, ethanol (pure) and methanol (Laboratory reagent grade) from Fisher Scientific, terephthalic acid (>99%) from TCI Chemicals, nitric acid (65% solution) from ChemLab, terbium nitrate pentahydrate (99.9%) from Sigma Aldrich and europium nitrate hexahydrate (99.9%) All chemicals were used as received without any further purification steps.

Synthesis of BDC bioMOF. BDC bioMOF was synthesized analogously to bio-MOF-1.(An et al., 2009) Adenine (0.625 mmol) and terephthalic acid (1.25 mmol) were dissolved in 67.5 ml *N,N*-dimethylformamide (DMF) in a Schott pressure-plus synthesis bottle. Upon addition of zinc acetate dihydrate (1.875 mmol) in 10 mL deionized water, a white precipitate was formed. This first precipitate was dissolved by adding 695 µL of 65% nitric acid (5 mmol). The resulting transparent synthesis solution was stored at 130°C for 24 h. The resulting powder was recovered by vacuum filtration, washed in 50 mL fresh DMF (3x) and subsequently in 50 mL fresh methanol (3x), before being air dried for 6 h at room temperature and finally overnight at 80°C.

RE-loading. Washed and dried BDC bioMOF was soaked in pre-made M^{3+} solutions in *N,N*-dimethylformamide (DMF) (0.05 M) for seven days under continuous shaking on a Heidolph Unimax 1010 platform shaker at 350 rpm. Fresh cation exchange solution was added daily after removal of the solid by centrifugation. The resulting cation-exchanged material was washed with fresh DMF (2x) and methanol (2x), removed by filtration, air dried and finally dried overnight at 80°C.

Silver loading. Washed and activated BDC bioMOF (250 mg) was soaked in a solution of 43.7 mg $AgNO_3$ (25 mM) in 10 mL methanol. The suspensions were agitated overnight (16 h) on a Heidolph Unimax 1010 platform shaker at 350 rpm. The powders were collected using vacuum filtration, subsequently air-dried while stored in darkness for further analysis.

LED device fabrication: An indium-tin-oxide (ITO)-coated glass (~ 109 Ω cm) was used as substrate. Before use, the glass was washed by immersion and sonication for 10 min in following solvents: 1) alkaline-detergent water (Hellmanex solution), water, acetone and isopropanol. The cleaned ITO-glasses were treated in an ultraviolet-ozone reactor (30 min) to lower the work function of the ITO layer. After that, a solution of the hole-injection layer, poly(3,4-ethylenedioxythiophene):polystyrene (PEDOT:PSS; Sigma Aldrich, high conductivity), was spin coated at 3000 rpm for 120 seconds and subsequently annealed at 150ºC during 15 minutes. Next, a solution of polymer (PS: Mn~250000 $g \cdot mol^{-1}$) in chlorobenzene (Sigma Aldrich, anhydrous), with 5% wt of the selected (M^{x+}) BDC bioMOF, was spin coated for 60 seconds at 1000 rpm and annealed at 80ºC for 15 minutes. Finally, a 150 nm aluminum (Al) electrode layer was vapor deposited on top of the emissive layer.

Structural characterization. Powder X-ray diffraction (PXRD) patterns were recorded at room temperature on a STOE STADI MP in Bragg-Brentano mode (2θ - θ geometry; CuKα1, 1.54060 Å) using a linear position sensitive detector to confirm the crystallinity and structure of all synthesized materials after activation for 24 h in air at 100 °C. Structure refinement was based on eight scans in capillary mode, summed to minimize the signal-to-noise ratio. Structural refinement was performed with TOPAS software. Continuous rotation electron diffraction (cRED) data were collected using a JEOL JEM-2100 transmission electron microscope (TEM) operated at 200 kV using a Gatan Cryo-transfer tomography holder (914). The sample powder was gently crushed in an agate mortar and dispersed in absolute ethanol. Then, a droplet of the suspension was transferred onto a holey carbon film covered copper grid. Data collection was performed using liquid nitrogen cooling at 96 K. Diffraction patterns were collected during continuous tilting of the goniometer using a high-speed hybrid detection camera (Timepix Quad). Data collection was performed using the Instamatic software package, with an integrated routing to facilitate crystal tracking during crystal tilting. (J. Appl. Cryst. (2018). 51, 1652-1661) Collected datasets were processed and merged using X-ray Detector Software (XDS) (Acta Crystallogr. Sect. D. Biol. Crystallogr. 2010, 66, 133-

144) to create the hkl file used for the structure determination. In order to increase data completeness three data sets were merged. The structure of BDC bioMOF could be solved from individual data sets as well as merged data using the software SHELXT.(Sheldrick, 2008) Refinements were performed using SHELXL,(Sheldrick, 2008) for details regarding the structure refinement, see Table S-3.1. An example electron diffraction image of BDC bioMOF is shown in Figure S-3.1.

Rietveld Refinement. After a structural model was obtained from electron diffraction data, it was Rietveld refined against powder X-ray diffraction data recorded at 298 K using TOPAS Academic v6. The background was fitted using a 12-term Chebyshev polynomial combined with a 1/x background function to take into account air scattering contributions at low angles. Peak shapes were fitted using the modified Thompson-Cox-Hastings pseudo-Voigt function convoluted with Topas's 'Simple_Axial_Model' macro account for axial divergence. In a first, it quickly became apparent that the initial model did not account for all observed intensity in the powder pattern. Fourier mapping indeed revealed additional electron density present in the one-dimensional channels, which was modeled and subsequently freely refined as 4 water molecules. Both Zn sites were freely refined, while for the μ2-O site only its y-coordinate was refined to keep it on the 2-fold rotation axis. The linkers were refined as rigid bodies. Table S2 provides a summary of the Rietveld refinement, whereas Figure S1 shows the asymmetric unit.

Solid—state nuclear magnetic resonance (NMR) measurements were performed on a 600 MHz Varian NMR spectrometer equipped with a 1.6 mm Varian HXY FastMAS probe. Magic-angle spinning (MAS) frequency was set to 40 kHz during all experiments. Larmor frequencies for ^{1}H and ^{13}C were 599.48 and 150.76 MHz respectively. Both ^{1}H and ^{13}C frequency axes were calibrated against tetramethylsilane.

1H and ^{13}C MAS NMR spectra were collected using the Hahn-echo pulse sequence with the 90° pulse lengths of 1.5 μs and the inter-pulse delays of 25 μs. The numbers of accumulated scans were 8 and 1800 with the recycle delays of 5 and 120 s for 1H and ^{13}C, respectively.

Two-dimensional ^{1}H-^{13}C heteronuclear correlation (HETCOR) NMR spectra were obtained by first exciting the ^{1}H nuclei with a 90° pulse of 1.5 µs and allowing their magnetization to evolve for t1. After that, the magnetization was transferred to ^{13}C nuclei by a 4.0 ms CP block for ^{13}C acquisition. Simultaneously, high-power XiX heteronuclear decoupling was applied to the ^{1}H channel. A total of 4 500 scans were acquired for each of the 20 increments along the indirectly detected dimension. This experiment was carried out in hypercomplex mode. In the case of ^{1}H-^{13}C Lee-Goldburg heteronuclear correlation (LG-HETCOR)(Van Rossum et al., 2000) experiments, additional 0.6 µs ^{1}H tilt pulse was employed prior to the 0.1 ms LG-CP transfer. These experiments consisted of 12 increments with 1 024 scans each.

For proton spin-diffusion (PSD) measurements, 100 increments in the indirect dimension were collected with 16 scans per increment and repetition delay of 1 s. Eighteen such two-dimensional spectra were recorded with spin-diffusion mixing times ranging from 0 to 100 ms. During the mixing period a radio-frequency driven recoupling (RFDR) (Bennett et al., 1998) was employed.

Physicochemical and optical characterization. Fourier transform infrared spectroscopy (FTIR) spectra were recorded on a Bruker IFS 66v/S spectrometer. Thin transparent wafers of KBr mixed with 1 wt% of sample were prepared. Scanning electron microscopy (SEM) micrographs were recorded using a JEOL-6010LV SEM after depositing a palladium/gold layer on the samples using a JEOL JFC-1300 autofine coater under Ar plasma. Thermogravimetric analysis (TG) was performed using a TA Instruments Q500 thermogravimetric analyzer. The samples were treated under an oxygen flow with a linear heating ramp of 5°C/min to 650 °C. TA Universal Analysis software was used for post-measurement data handling. Inductively coupled plasma (ICP) mass spectrometry was performed to determine the metal contents of the powders using an Agilent ICP-MS 7700X. 50 mg of the activated MOF powders was digested in a mixture of 0.5 mL 65% HNO_3 and 3 mL solution of 40% HF in water. X-ray Photoelectron Spectroscopy (XPS) was performed on a Thermo Scientific™ K-Alpha™ X-ray Photoelectron Spectrometer System with

an Al-Kα source producing x-rays with energy hν = 1486.7 eV that are focused to a 200 x 200 μm² spot. An electron flood gun was applied during the XPS measurements to minimize charging effects.

Excitation-emission spectra were measured using a FLS 920 fluorescence spectrophotometer (Edinburgh Instruments, Photonics division) at different excitation wavelengths from 250 to 600 nm with 5 nm intervals. For each excitation wavelength, the emission (280-800 nm) was collected starting 30 nm above the excitation wavelength. For UV excitation, the emission signal above 405 nm was measured using a 400 nm long pass glass filter to avoid second order excitation interference and the collected signal was corrected for the transmittance of this filter. These emission spectra were compiled using Matlab to form two-dimensional emission-excitation profiles, where the raw data were interpolated to a 1 nm x 1 nm resolution and corrected for noise and background. Diffuse Reflectance Spectroscopy (DRS) was recorded using a Lambda 950 UV-VIS spectrophotometer (PerkinElmer). BaSO4 powder was used as a reference in the wavelength range of 200 to 800 nm. Stationary electroluminescence measurements were recorded using an Edinburgh FLS 980 fluorimeter where the Xe-lamp (usually for optical excitation) was blocked in order to only register the electroluminescence spectra. Current – Voltage (I-V) curves were measured in the dark at room temperature using a Keithley 2400 device.

RESULTS

Table S1: Continuous rotation electron diffraction (cRED) and structure determination details of as-synthesized BDC bioMOF.

	Merged data
Crystal system	Monoclinic
Space group	C2/c (n°. 15)
a, Å	15.19
b, Å	37.75
c, Å	9.74
α, °	90
β, °	102.45
γ, °	90
Volume, Å^3	5453.80

λ, Å	0.0251
Exposure time per frame (s)	0.6
Tilt speed (° s^{-1})	0.45
Completeness, %	89.4
Resolution, Å	0.99
Rint	0.2144
No. of symmetry independent reflections	2684
Parameters	144
Restraints	0
R1	0.3618

Table S2: Final parameters for the Rietveld refinement of BDC bioMOF.

Formula	**Zn4O9C31N15·O8**
Z	4
λ / Å	1.54016 (Cu Kα1)
T / K	298 K
Crystal system	Monoclinic
Space group	C2/c (n° 15)
a / Å	14.3293(10)
b / Å	36.4851(35)
c / Å	9.5597(09)
α / °	90
β / °	105.9773(77)
γ / °	90
V / Å³	4804.85
Rwp / %	7.714
Rexp / %	2.132
RBragg / %	3.994
GoF	3.619

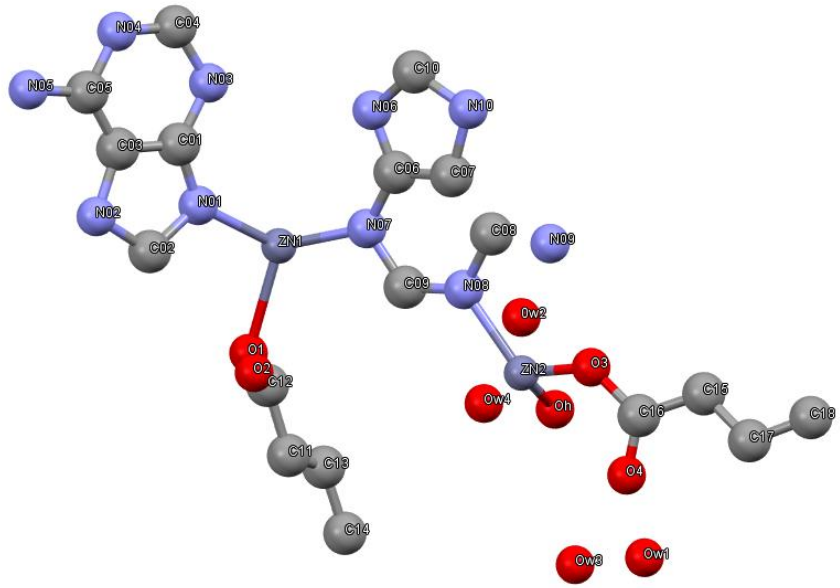

Figure S1: Asymmetric unit of BDC bioMOF

Table S3: List of atomic coordinates – structure obtained from cRED data

Atom	Label	*x*	*y*	*z*	occupancy
Zn	Zn1	0.56651	0.79502	0.43661	1
	Zn2	0.57304	0.64535	0.62646	1
C	C01	0.63358	0.82893	0.18469	1
	C02	0.74254	0.82864	0.39447	1
	C03	0.72768	0.76765	0.86523	1
	C04	0.71301	0.84703	0.1688	1
	C05	0.70701	0.7852	0.71572	1
	C06	0.66756	0.74978	0.93244	1
	C07	0.67847	0.72499	1.01798	1
	C08	0.5564	0.8404	-0.05885	1
	C09	0.72057	0.85881	0.03207	1
	C10	0.53306	0.53533	0.56484	1
	C11	0.54849	0.56993	0.59684	1
	C12	0.56927	0.50505	0.62242	1
	C13	0.54217	0.46955	0.58312	1
	C15	0.4953	0.7275	0.2317	0.5
	C16	0.49314	0.69049	0.20302	0.5
	C17	0.50813	0.6659	0.31766	0.5
	C19	0.54799	0.71847	0.48495	0.5
	C20	0.449	0.71655	-0.00912	0.5
N	N01	0.64996	0.81706	0.31885	1
	N02	0.78673	0.84287	0.29861	1
	N03	0.54942	0.82651	0.0744	1
	N04	0.63741	0.85625	-0.0774	1
	N05	0.7961	0.87572	-0.00103	1
	N06	0.46761	0.74382	0.10617	0.5
	N07	0.5279	0.74344	0.37287	0.5
	N08	0.53994	0.68168	0.45756	0.5
	N09	0.5045	0.62869	0.30591	0.5
	N10	0.4525	0.6835	0.05032	0.5
O	O1	0.61951	0.78467	0.64486	1
	O2	0.52394	0.60024	0.53819	1
	O3	0.604	0.57511	0.7375	1
	O4	0.75649	0.81299	0.71321	1
	O5	0.5	0.66005	0.75	1

Table S4: List of atomic coordinates – structure Rietveld refined from powder X-ray diffraction data

Atom	Label	*x*	*y*	*z*	occupancy
Zn	Zn1	0.5617	0.7946	0.4504	1
	Zn2	0.5736	0.6426	0.6106	1
C	C01	0.63358	0.82893	0.18469	1
	C02	0.74254	0.82864	0.39447	1
	C03	0.71301	0.84703	0.1688	1
	C04	0.5564	0.8404	-0.05885	1
	C05	0.72057	0.85881	0.03207	1
	C06	0.4953	0.7275	0.2317	0.5
	C07	0.49314	0.69049	0.20302	0.5
	C08	0.50813	0.6659	0.31766	0.5
	C09	0.54799	0.71847	0.48495	0.5
	C10	0.449	0.71655	-0.00912	0.5
	C11	0.7298	0.76281	0.85441	1
	C12	0.70839	0.77514	0.7007	1
	C13	0.65697	0.76202	0.92628	1
	C14	0.67729	0.74951	1.07035	1
	C15	0.53944	0.53243	0.5694	1
	C16	0.57861	0.56698	0.63796	1
	C17	0.56729	0.49886	0.63805	1
	C18	0.52775	0.4666	0.56868	1
N	N01	0.642	0.8205	0.327	1
	N02	0.792	0.8460	0.294	1
	N03	0.54942	0.82651	0.0744	1
	N04	0.63741	0.85625	-0.0774	1
	N05	0.7961	0.87572	-0.00103	1
	N06	0.46761	0.74382	0.10617	0.5
	N07	0.5279	0.74344	0.37287	0.5
	N08	0.53994	0.68168	0.45756	0.5
	N09	0.5045	0.62869	0.30591	0.5
	N10	0.4525	0.6835	0.05032	0.5
O	O1	0.639	0.8047	0.690	1
	O2	0.7625	0.76672	0.62818	1
	O3	0.562	0.5985	0.557	1
	O4	0.62408	0.56885	0.7657	1
	Oh	0.5	0.6460	0.75	1
H_2O	Ow1	0.930	0.4760	0.701	1
	Ow2	0.733	0.5891	0.320	1
	Ow3	0.854	0.5459	0.836	1
	Ow4	0.868	0.5844	0.456	1

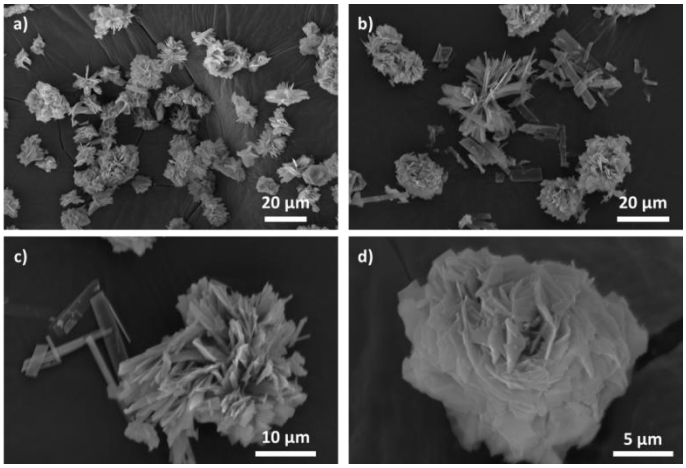

Figure S2: Scanning electron microscopy images of bio-MOF BDC show strongly intergrown platelet crystals.

BDC bioMOF consists of infinite two-dimensional layers, stacked by rows of terephthalate linkers (BDC_B), ultimately yielding one-dimensional channels along the c-axis of approximately 10 Å in diameter (Figure S3c). The layers feature a complex architecture involving two distinct Zn^{2+} dimers (Zn_1-Zn_1 and Zn_2-μ_2O-Zn_2), two distinct adeninate linkers (1:2 ratio Ad_A:Ad_B) and one terephthalate linker (BDC_A). The basic building unit in these layers is formed by a first dimer of two symmetry-equivalent Zn_1^{2+} ions (Figure S4a) interconnected by three adeninate linkers: one Ad_A molecule and two symmetry-equivalent Ad_B molecules. A two-fold symmetry axis runs through Ad_A, rendering it crystallographically disordered over two positions, which eliminates the distinction between Zn_1-N_3 / Zn_1-N_9 and between Zn_2-N_1 / Zn_2-N_7. Remarkably, adeninate features two different coordination modes within BDC bioMOF (i.e. Ad_A and Ad_B), which were previously only observed in separate structures. A single carboxylate oxygen atom from the intralayer terephthalate (BDC_A) completes the tetrahedral coordination environment around each Zn_1 ion. These BDC_A linkers connect each trigonal bipyramidal $(Zn_1)_2(Ad)_3$ unit to two others in an infinite chain that adopts a zig-zag motif with the Ad_A linker alternating between an up and down orientation (Figure S4b). Note that BDC_A's carboxylate group assumes a monodentate coordination to Zn_1, as has been reported in other adeninate MOFs.(Sushrutha et al., 2016). To form the layer, neighboring chains are knitted together by a second inorganic unit, consisting of two symmetry-equivalent Zn_2^{2+} ions interconnected by a μ_2-O group (Figure S5a). Each Zn_2 adopts a tetrahedral geometry and is coordinated by an Ad_B linker and an Ad_A from a $(Zn_1)_2(Ad)_3$ unit in a chain adjacent to the one of the Ad_B ligand. Each Zn_2 thus connects two neighboring chains. The μ_2-O group then connects these two chains to the next two through the second Zn_2 ion in the dimer (Figure S5b). Finally, the layers are connected by BDC_B linkers through coordination of single carboxylate oxygen atoms with the Zn_2 ions. The BDC_B connections are presumably strengthened by hydrogen bond interactions between the carboxylates and the neighboring -NH_2 groups of Ad_A (< 2.5 Å) and Ad_B (< 3 Å).

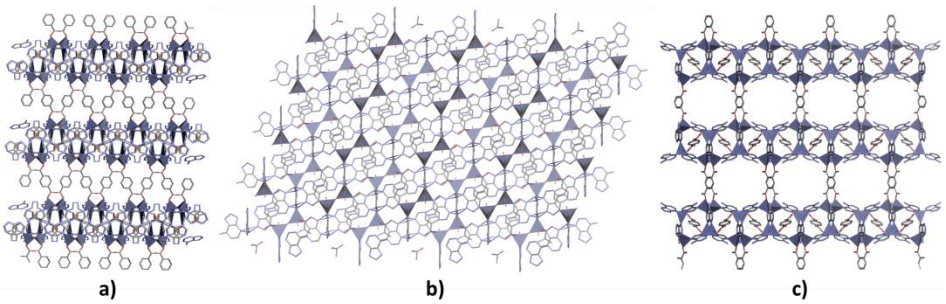

Figure S3: Crystallographic representation of BDC bioMOF along a) [100], b) [010] and c) [001] crystallographic axes.

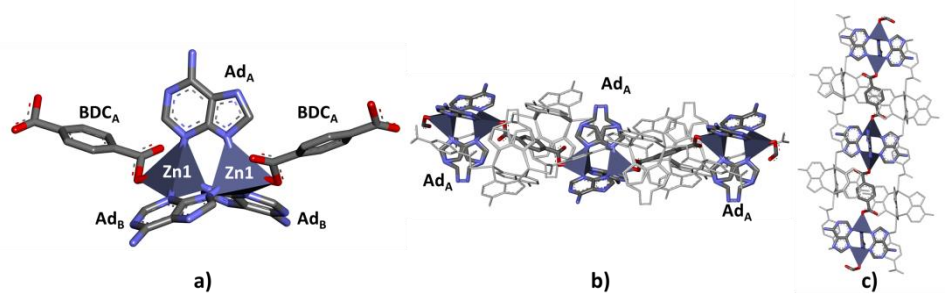

Figure S4: Crystallographic representation of a) trigonal bipyramidal coordination around the Zn_1 dimer by one Ad_A, two symmetry-equivalent Ad_B and one BDC_A; b-c) infinite intralayer zig-zag chain of $(Zn_1)_2(Ad)_3$ units with BDC_A along [201]. Other molecules are presented in grayscale for clarity. Zn_1 = purple, C = grey, O = red, N = blue.

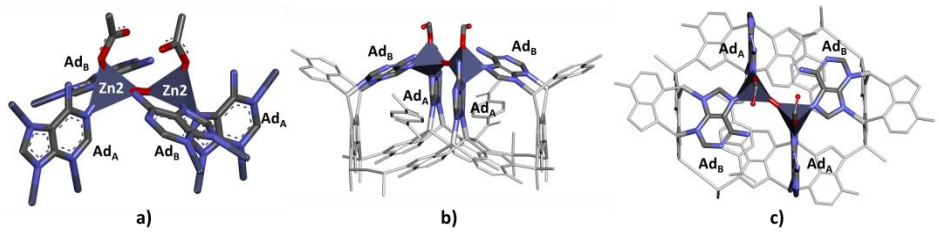

Figure S5: Crystallographic representation of a) coordination around the Zn_2 dimer by one Ad_A, one Ad_B, a μ_2-O and a carboxylate from BDC_B; b-c). Other molecules are presented in grayscale for clarity. Zn_2 = purple, C = grey, O = red, N = blue

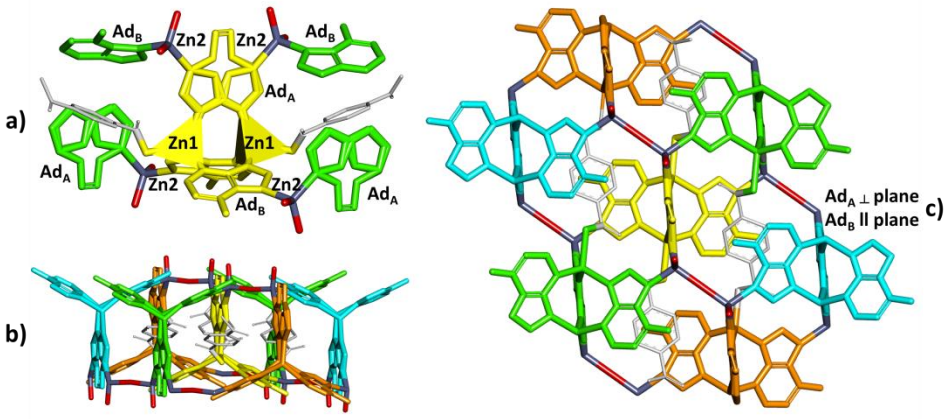

Figure S6: Crystallographic representation of a) $(Zn_1)_2(Ad)_3$ unit (yellow) connection to Zn_2 through its Ad_A or Ad_B; b) connectivity of $(Zn_1)_2(Ad)_3$ to the $(Zn_1)_2(Ad)_3$ units in the neighbouring chains (green – orange - aquamarine). Note that BDC_A is shown in greyscale for clarity.

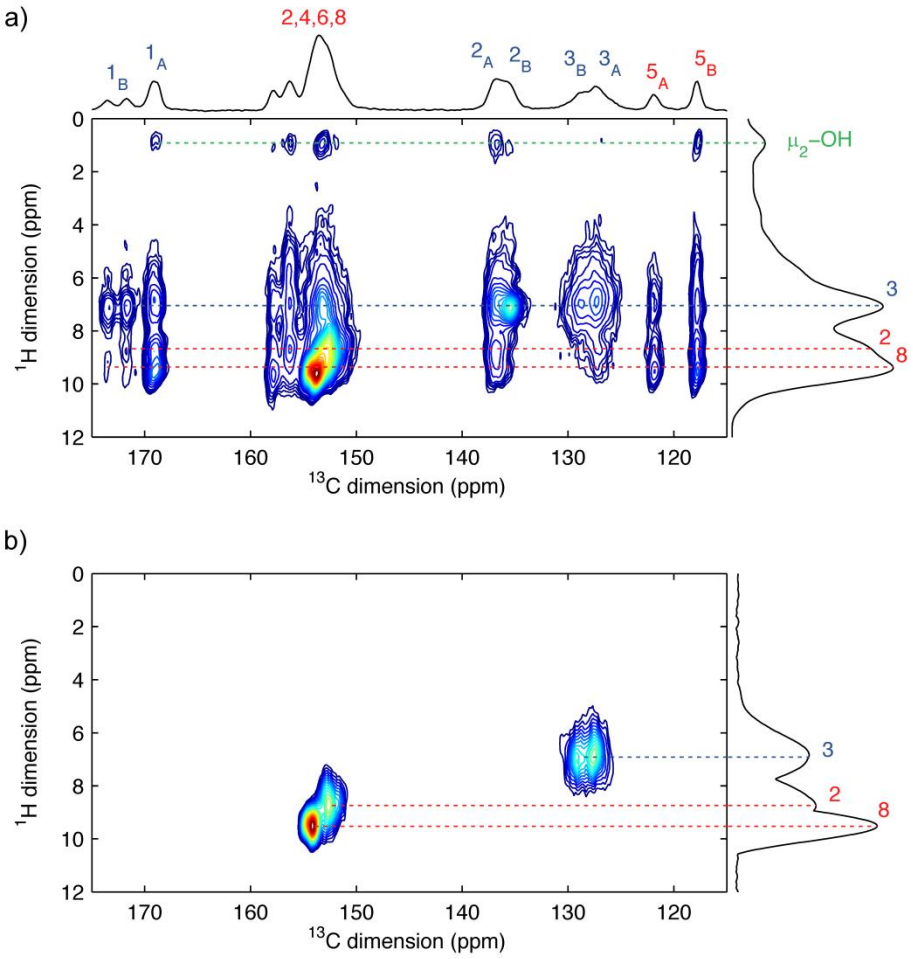

Figure S7: Two-dimensional ^{1}H-^{13}C HETCOR (a) and LG-HETCOR (b) NMR spectra, which support the assignment of the ^{13}C and ^{1}H signals. The first rough assignment of the signals was carried out using chemical-shift prediction algorithms of ACD-Lab. Further assignment to BDC_A, BDC_B, Ad_A and Ad_B followed from the HETCOR spectrum: BDC and Ad carbon nuclei, which are closer in space to μ_2-OH protons, exhibit stronger cross peaks at 1 ppm in the indirect dimension (marked by green dotted line). Finally, the LG-HETCOR spectrum showed that the H2 protons of both Ad_A and Ad_B contribute to the ^{1}H signal at 8.8 ppm, and the H8 protons of both Ad_A and Ad_B contribute to the ^{1}H signal at 9.6 ppm.

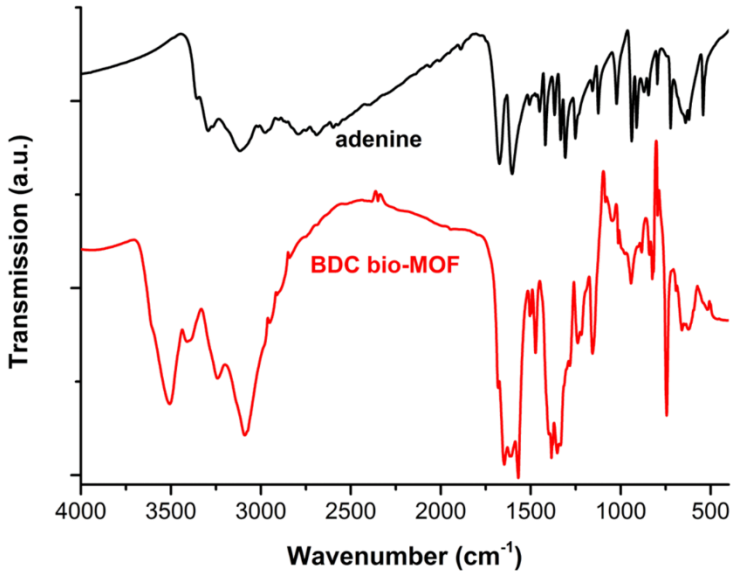

Figure S8: Fourier-transformed infrared spectra of adenine (black) and bio-MOF BDC (red).

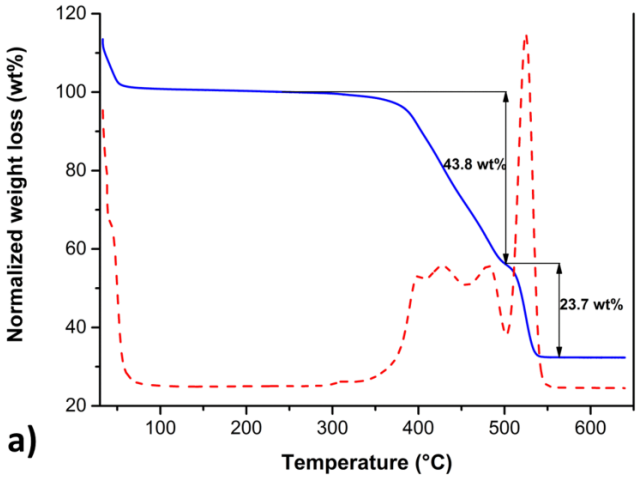

Figure S9: Thermogravimetric (TG) analysis of BDC-bioMOF. Weight loss (blue) and 1st derivative signal (red) under O_2 gas, heating at 5 °C/min.

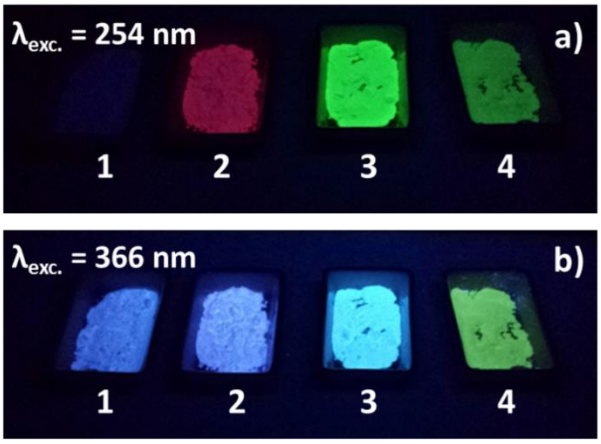

Figure S10: Photographs of BDC bioMOF powders under UV illumination, (a) 254 nm and (b) 366 nm for (1) BDC bioMOF, (2) Eu^{3+}-loaded, (3) Tb^{3+}-loaded and (4) Ag^{+}-loaded

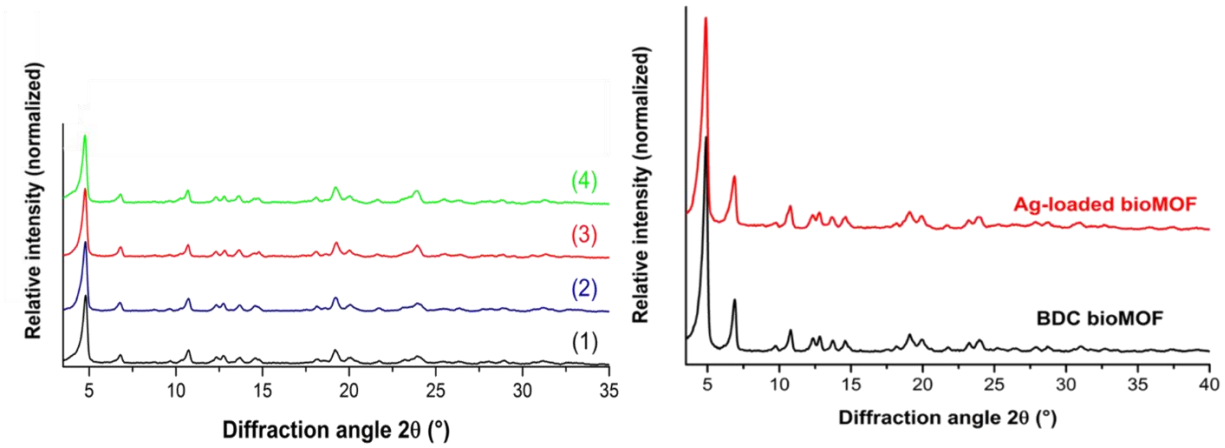

Figure S11: Powder X-ray diffraction patterns of as synthesized BDC bioMOF (1), water stability (2), and Eu^{3+}-loaded (3), Tb^{3+}-loaded (4) (left) and Ag^{+}-loaded bioMOF (right).

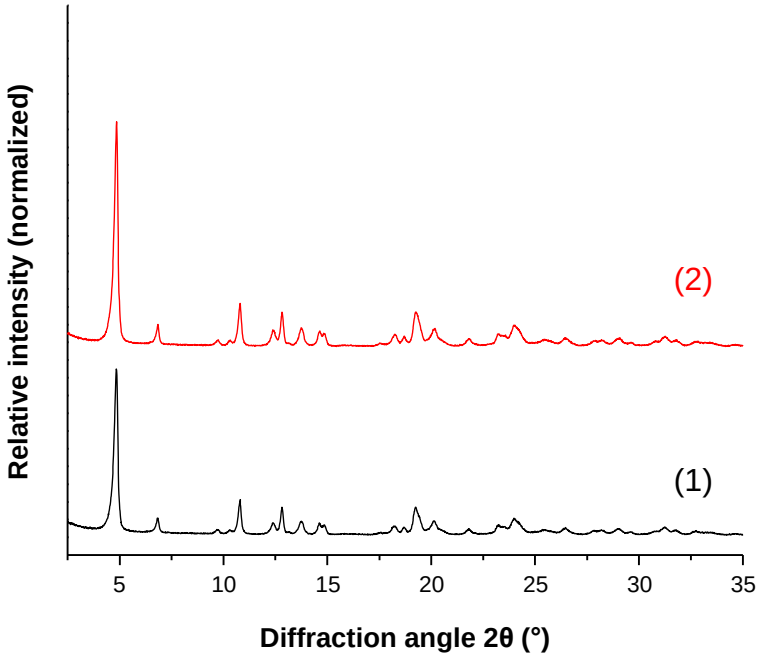

Figure S12: Powder X-ray diffraction patterns of water exposed Tb^{3+}-loaded BDC bioMOF (1) and water exposed Eu^{3+}-loaded BDC bioMOF (2). No differences were observed when compared to the diffractograms of the as synthesized MOFs, indicating that the structure is stable in the presence of water.

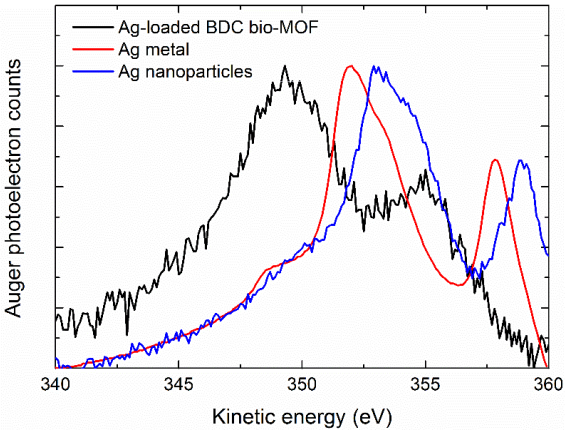

Figure S13: Silver Auger spectra recorded by XPS of Ag-loaded BDC (black), an evaporated thin-film of silver metal (red), and 10 nm sodium citrate-stabilized silver nanoparticles (blue).

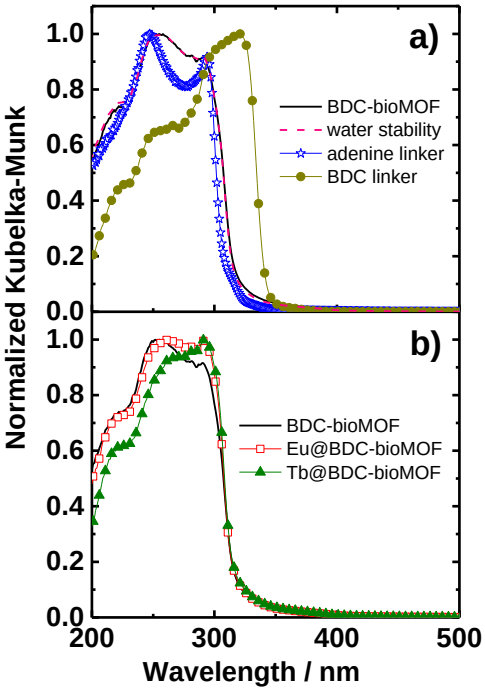

Figure S14: a) Comparison between the DRS spectra of BDC-bioMOF, BDC-bioMOF in water treatment, BDC linker and adenine linker. b) DRS spectra of doped and undoped BDC-bioMOF.

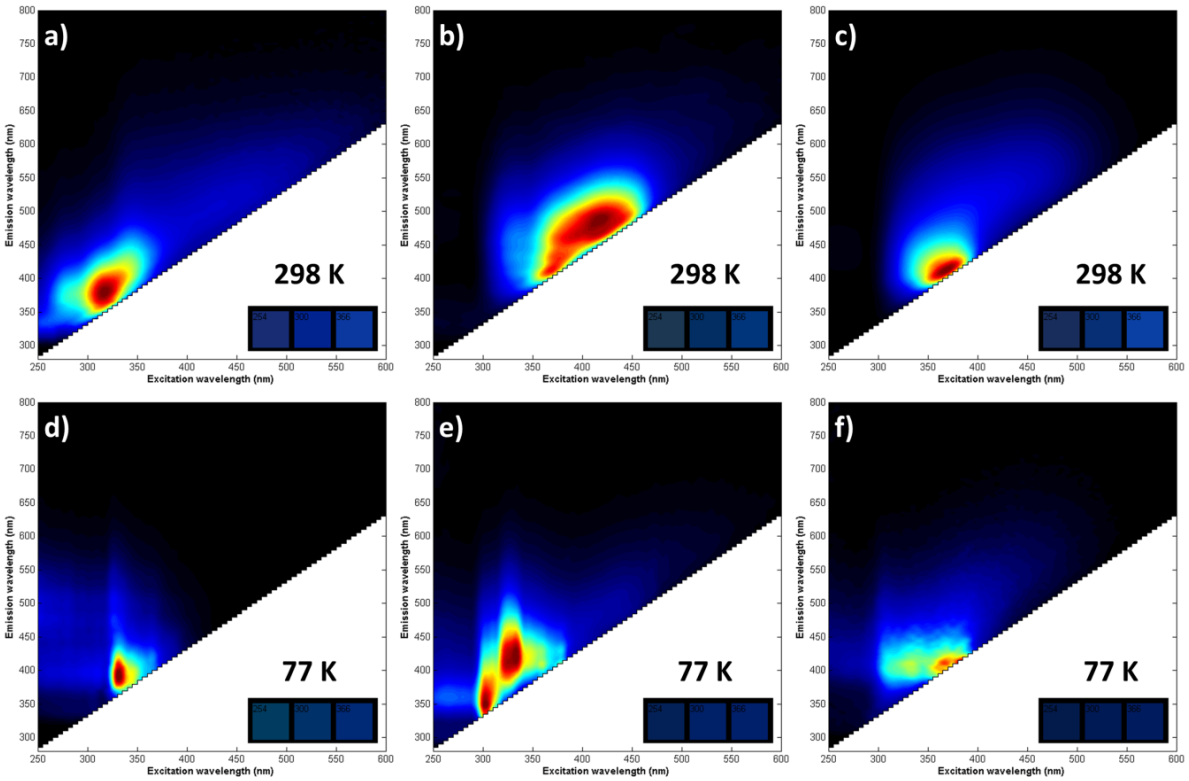

Figure S15: Excitation/emission plots of (a&d) 1,4-H_2BDC, (b&e) adenine and (c&f) BDC bioMOF at room temperature (a-c) and 77 K (d-f).

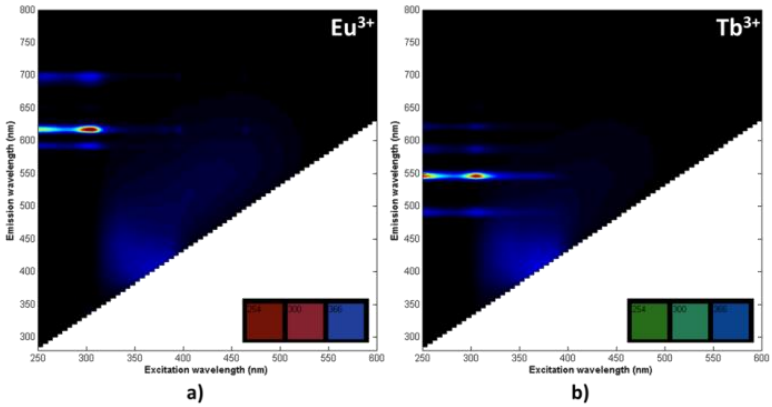

Figure S16: Fluorescence excitation-emission (x-y) maps of BDC bio-MOF loaded with (a) $Eu^{3+}$and (b) Tb^{3+}**.**

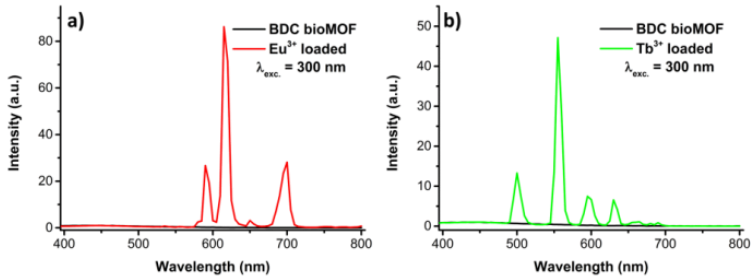

Figure S17: Emission spectra of RE-loaded BDC bio-MOF; (a) $Eu^{3+}$and (b) Tb^{3+}.

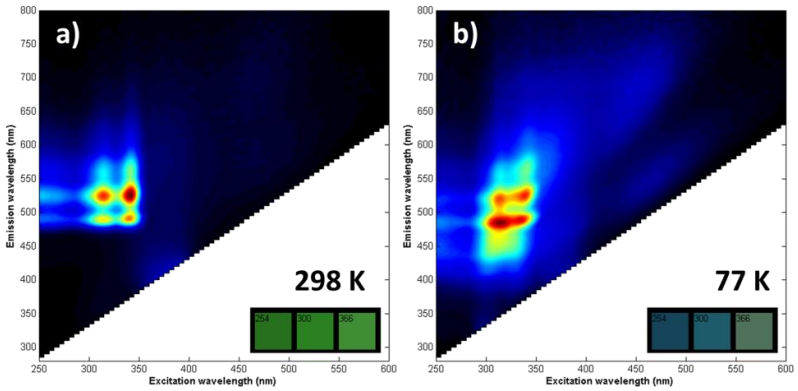

Figure S18: Fluorescence excitation-emission (x-y) maps of BDC bio-MOF after Ag^{+}-loading (a) at 298 K and (b) 77 K.

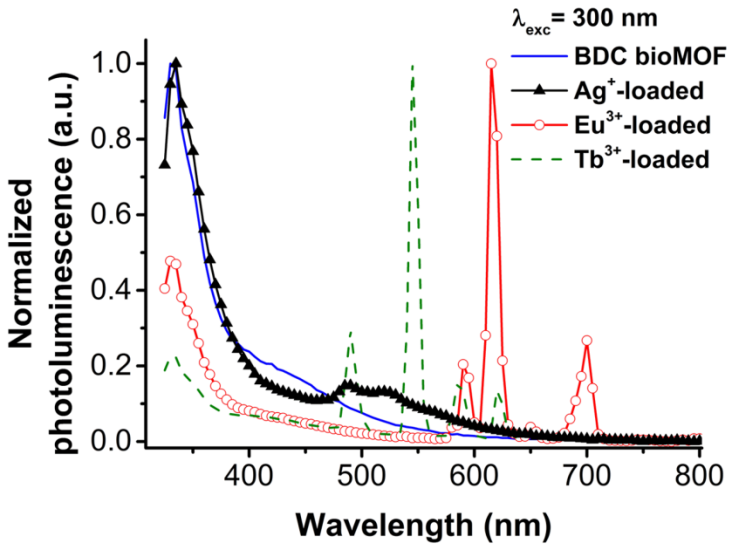

Figure S19: Comparison of the photoluminescence (PL) spectra of M^{x+}-loaded BDC bioMOFs (M^{x+}=Ag^{+}, Eu^{3+} and Tb^{3+}) in polystyrene matrix.

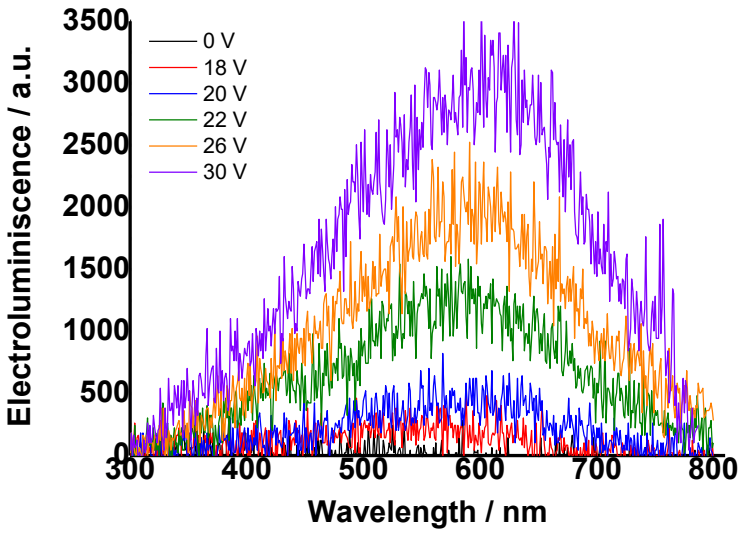

Figure S20: Electroluminescent spectra of undoped BDC-bioMOF under different applied voltages.